Preprints of the 23rd IFAC World Congress
Busan, Republic of Korea, August 23-28, 2026

Robust reset control design by loop shaping for piezoelectric-actuated positioner in presence of nonlinearity ⋆

A. Sebghati * **S. H. HosseinNia** *

* *Precision and Microsystems Engineering Department, Faculty of ME, TU Delft (e-mail: a.sebghati@tudelft.nl; s.h.hosseinniakani@tudelft.nl)*

Abstract: Loop shaping is widely used in precision motion control, but conventional approaches, focused on phase margin and open-loop gain, are inadequate for piezo positioning systems where open-loop phase critically affects performance. This paper proposes generalized loop-shaping guideline tailored for nonlinear piezo-actuated stages. A constant-in-gain lead-in-phase reset controller is developed to implement the guideline by overcoming waterbed effect in linear control. An intuitive methodology for shaping filter design is presented to ensure reliable reset control implementation. Using (higher-order) sinusoidal input describing functions, nonlinear motion control is designed. Experiments demonstrate closed-loop bandwidth flatness (± 1 dB) and enhanced sensitivity function.

Keywords: Loop shaping, Reset control, Shaping filter, Describing function, Piezo stage

1. INTRODUCTION

Loop-shaping is a well-established frequency-domain methodology for linear control design, widely applied in precision motion systems to achieve high performance (precision and bandwidth) and stability margins, as reflected by the closed-loop and sensitivity functions. Traditionally, it focuses on the open-loop phase near the crossover frequency ω_c to ensure robust stability and desirable transient characteristics (characterized by phase-margin constraint), while performance is tuned via ω_c and the open-loop gain shaping (see, e.g., Schmidt et al. (2020)). Unfortunately, this traditional approach is not adequate for ultra-precision motion systems.

In piezo-actuated positioners with high stiffness and lightly-damped resonance, open-loop phase is also critical for performance where open-loop gain unavoidably remains close to unity over a wide frequency range around ω_c (unity gain crisis not captured by conventional methods) due to performance-stability trade-offs. For piezoelectric stages, offering superior precision and bandwidth (BW) over electromagnetic actuators (see, e.g., Ru et al. (2016)), a flatness of ± 1 dB in the closed-loop response in addition to the maximum possible ω_c is typically desired, which conventional loop-shaping struggles to achieve due to missing open-loop phase shaping in frequency range of crisis.

This work shows that shaping the open-loop phase over a wide frequency range without altering the gain can extend ω_c while preserving the flatness constraint. However, such phase enhancement requires a constant-in-gain lead-in-phase (CgLp) filter, unavailable in linear control. Reset control, introduced by Clegg (1958), serves as one of the control types (see, e.g., Heertjes et al. (2023) for another type) that provides a nonlinear means to overcome this limitation (see, e.g., Beker et al. (2002); Heertjes et al. (2016); Zhao et al. (2019)). CgLp reset control closely approximates this property and has enabled high-performance motion control, thanks to the recently developed analytical frequency-domain tools (see, e.g., Saikumar et al. (2021)). Although reset element is nonlinear (see, e.g., Zhao et al. (2013)), recent advancements have enabled reset control design by loop shaping. The phase advantage can be analyzed via the sinusoidal input describing function (SIDF), though higher-order SIDF (HOSIDF) analysis reveals limitations due to the generated higher-order harmonics in feedback characterized by multiple resets per cycle (Zhang and HosseinNia (2024b)). Shaping filters (Karbasizadeh et al. (2022); Zhang and HosseinNia (2024a)) can mitigate these effects, though generalized design guidelines remain lacking.

Nonlinearities in piezo actuators, e.g., hysteresis and amplifier saturation, further limit achievable performance in a large travel range (see, e.g., Zhong and Yao (2008)). Feedforward compensation can reduce but not eliminate these effects (Sabarianand et al. (2020); Esbrook et al. (2012)). Thus, there is a need to a robust motion control to preserve performance against the nonlinearities. Although measured frequency response generally represents linear dynamics, the HOSIDF (Nuij (2007)) provides a means to characterize such nonlinearities as frequency-domain uncertainties. However, HOSIDF measurement of piezo systems remains unexplored (Alferink et al. (2025)).

This paper integrates loop-shaping theory, practically effective reset control, and nonlinear analysis as follows:

- New loop-shaping guideline enabling high ω_c and flat closed-loop response (± 1 dB) even if the open-loop gain is near unity in a wide frequency range;

⋆ Financed by Physik Instrumente SE & Co. KG and co-financed by Holland High Tech with PPS Project supplement for research and development in the field of High Tech Systems and Materials.

©2026 the authors. Accepted by IFAC for publication under a Creative Commons Licence CC-BY-NC-ND

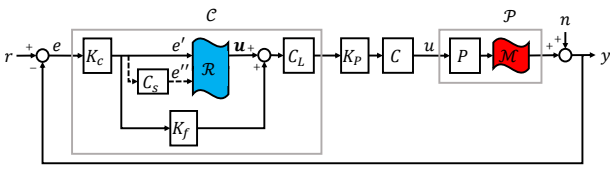


Fig. 1. Control loop with linear and nonlinear elements.

- Extension to uncertain systems;
- CgLp reset control with a generalized shaping-filter synthesis method for viable open-loop phase shaping;
- Real HOSIDF measurements to represent piezo actuators' nonlinearities in frequency domain.

2. PRELIMINARIES

The feedback control structure is considered as Fig. 1. The piezo stage is given by the uncertain dynamics $\mathcal{P}$:

$$\mathcal{P}(j\omega) = P(j\omega).\mathcal{M}(j\omega) \tag{1}$$

where P and $\mathcal{M}$ respectively denote the measured frequency response and multiplicative uncertainty for small and large travel ranges. $\mathcal{M}$ is obtained by the ratio between P and the 1st-order SIDF (SIDF for brevity), assuming that the HOSIDFs are negligible. Hence, $\mathcal{P}$ is represented by an uncertain region in the Bode plane that contains P.

C denotes linear control with the unity DC gain. K_P is used to set the cross-over frequency ω_c. $\mathcal{C} = 1$ is selected to represent a scenario of linear motion control; otherwise, $\mathcal{C}$ denotes the constant-in-gain lead-in-phase (CgLp) reset control for a scenario of nonlinear motion control.

The generalized first-order reset element (GFORE) $\mathcal{R}$ below constructs the CgLp reset control:

$$\begin{cases} \dot{\boldsymbol{x}}(t) = -\omega_r' \boldsymbol{x}(t) + \omega_r' e' & \text{if } e''(t) \neq 0 \\ \boldsymbol{x}(t^+) = \gamma \boldsymbol{x}(t) & \text{if } e''(t) = 0 \\ \boldsymbol{u}(t) = \boldsymbol{x}(t) \end{cases} \tag{2}$$

where $e', \boldsymbol{x}, \boldsymbol{u} \in \mathbb{R}$ respectively denote the input, state and output of the reset element. e'' is produced by the shaping filter C_s that is used for the resetting condition. The shaping filter lets bandpass the control nonlinearity in the required frequency range (see, e.g., Karbasizadeh et al. (2022)). The hybrid dynamics of the reset control consists of the base linear and switching dynamics $\mathcal{R}_{\text{bl}}$ and $\mathcal{R}_{\text{r}}$, represented by the first and second differential equations in (2) respectively. $\omega_r' \in \mathbb{R}_{++}$ is the corner frequency of the base linear dynamics and $\gamma \in (-1, 1) \subset \mathbb{R}$ is the resetting coefficient of the switching dynamics.

The (HO)SIDF $\mathcal{R}_1$ and $\mathcal{R}_n$ of (2) are given by Guo et al. (2009); Hou et al. (2020); Zhang and HosseinNia (2025):

$$\begin{aligned} &\mathcal{R}_1(j\omega) = \frac{1}{j\frac{\omega}{\omega_r'} + 1}.(1 + j\Theta_N), \\ &\mathcal{R}_n(j\omega) = \begin{cases} \frac{1}{j\frac{n\omega}{\omega_r'} + 1}.j\Theta_N e^{j(n-1)\angle C_s} & \text{if } n: \text{odd} \\ 0 & \text{if } n: \text{even} \end{cases}, \\ &\Theta_N = \hat{\Theta}.\Theta_s, \ \ \hat{\Theta} = \frac{2\omega(1-\gamma)(1+e^{-\frac{\pi}{\omega}\omega_r'})}{\pi(1+\gamma e^{-\pi\frac{\omega_r'}{\omega}})(\omega^2+\omega_r'^2)}, \\ &\Theta_s = e^{j\angle C_s}(\omega\cos(\angle C_s) + \omega_r'\sin(\angle C_s)) \end{aligned} \tag{3}$$

The SIDF of the nonlinear control $\mathcal{C}$ is calculated by:

$$\mathcal{C}_1(j\omega) = k_c.(\mathcal{R}_1(j\omega) + k_f).C_L(j\omega) \tag{4}$$

with the lead filter C_L and the gains k_c, k_f below such that $\mathcal{C}_1$ is CgLp (Hosseini et al. (2025)):

$$\begin{aligned} C_L(j\omega) &= \frac{j\frac{\omega}{\omega_r} + 1}{j\frac{\omega}{\omega_f} + 1}, \\ \omega_r &= \alpha\omega_r', \alpha = \sqrt{1 + \frac{16}{\pi^2}(\frac{1-\gamma}{1+\gamma})^2}, \\ k_f &= \frac{\omega_r}{\omega_f - \omega_r}, k_c = 1 - \frac{\omega_r}{\omega_f} \end{aligned} \tag{5}$$

The phase advantage from reset control is entangled with the cost of higher-order harmonics. For a reliable control design based on SIDF, zero-crossing more than two times per cycle, referred to as multiple reset, is not permitted. Shaping filter allows for tuning the phase advantage alongside frequency as a trade-off technique with the higher-order harmonics to ensure a reliable feedback control design. Shaping filter will be discussed in Section 5.1.

In linear motion control design, $\mathcal{C} = 1$, the sensitivity and complementary sensitivity functions S and T are given by

$$\begin{aligned} S(j\omega) &= \frac{1}{1 + L(j\omega)}, T(j\omega) = \frac{L(j\omega)}{1 + L(j\omega)}, \\ L(j\omega) &= K_P.C(j\omega).\mathcal{P}(j\omega) \end{aligned} \tag{6}$$

where L denotes the open-loop function. In nonlinear motion control design, unwanted higher-order harmonics are generated by reset control. It is first assumed that the higher-order harmonics have negligible effects on the performance during the control design process. Therefore, sensitivity and complementary sensitivity functions $\mathcal{S}_1$ and $\mathcal{T}_1$ below are considered (Saikumar et al. (2021)):

$$\begin{aligned} \mathcal{S}_1(j\omega) &= \frac{1}{1 + \mathcal{L}_1(j\omega)}, \mathcal{T}_1(j\omega) = \frac{\mathcal{L}_1(j\omega)}{1 + \mathcal{L}_1(j\omega)}, \\ \mathcal{L}_1(j\omega) &= \mathcal{C}_1(j\omega).K_P.C(j\omega).\mathcal{P}(j\omega) \end{aligned} \tag{7}$$

where $\mathcal{L}_1$ denotes the open-loop function based on the SIDF. Next, the frequency-domain tools pseudo- sensitivity and complementary sensitivity functions S_∞ and T_∞ below are used for validation (Saikumar et al. (2021)):

$$\begin{aligned} \mathcal{S}_\infty(j\omega) &= \max\{\Sigma_{i=1}^{\infty}|\mathcal{S}_i(j\omega,\kappa)|\sin(n\omega t + \angle\mathcal{S}_i(j\omega,\kappa))\}, \\ \mathcal{T}_\infty(j\omega) &= \max\{\Sigma_{i=1}^{\infty}|\mathcal{T}_i(j\omega,\kappa)|\sin(n\omega t + \angle\mathcal{T}_i(j\omega,\kappa))\} \end{aligned} \tag{8}$$

where $\mathcal{S}_n$, $\mathcal{T}_n$ capture the higher-order harmonics effects:

$$\begin{aligned} &\mathcal{S}_n(j\omega) = -\mathcal{T}_n(j\omega) = -S_{bl}(jn\omega).\mathcal{L}_n(j\omega). \\ &\frac{(\mathcal{S}_1(j\omega))^n}{|\mathcal{S}_1(j\omega)|^{n-1}}.\frac{(R(j\omega))^{n-1}}{|R(j\omega)|^{n-1}}, S_{bl}(j\omega) = \frac{1}{1 + L_{bl}(j\omega)}, \\ &L_{bl}(j\omega) = \mathcal{C}_{bl}(j\omega).K_P.C(j\omega).\mathcal{P}(j\omega), \mathcal{C}_{bl}(j\omega) = \\ &\mathcal{R}_{bl}(j\omega).C_L(j\omega), \mathcal{L}_n(j\omega) = \mathcal{C}_n(j\omega).K_P.C(jn\omega).\mathcal{P}(jn\omega) \end{aligned} \tag{9}$$

The base linear dynamics is indicated by *bl*. R denotes the Fourier series' coefficient of the sinusoidal reference. S_∞,T_∞ are representative of the all harmonics effects that must be close to S_1,T_1 to preserve the performance.

3. PROBLEM STATEMENT

3.1 Nano-positioning system

A piezoelectric-actuated nano-positioning stage of the type P-621.1CD PIHera is considered as a case study for motivation and experimental validation. It is equipped with a stack piezoelectric as the actuator with a stroke of $[-10, 120]$ μm. The laboratory setup is shown in Fig 2.

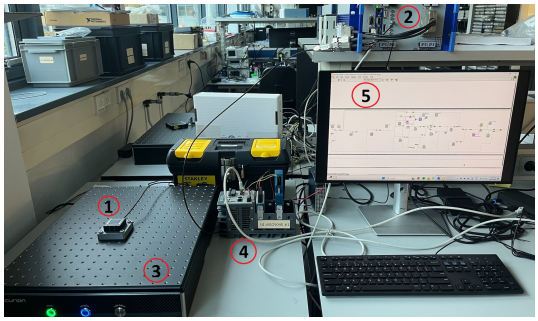


Fig. 2. Laboratory setup: (1) Piezoelectric stage with capacitor sensor, (2) E712, (3) Vibration isolation table, (4) CompactRio/FPGA, (5) Host computer.

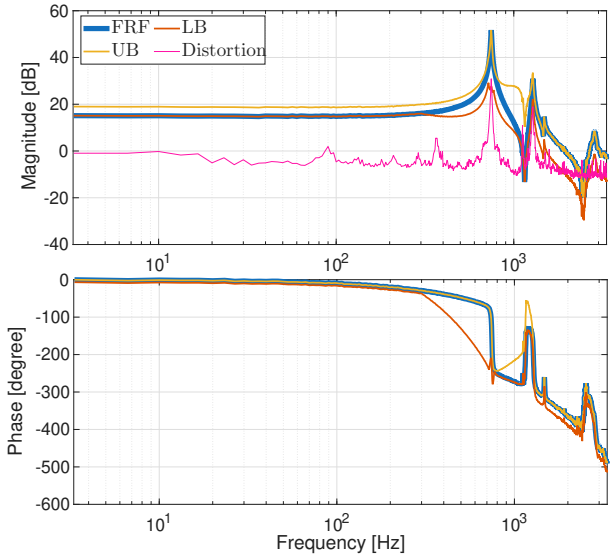


Fig. 3. Plant dynamics: Uncertain FRF

The plant's linear dynamics is identified by the measured frequency response function (FRF) in Fig. 3. A multi-sine input voltage is used at position 50μm with a travel range of 1 μm. A set of (HO)SIDF measurements returns that the $1^{\text{st}}-$order harmonic is dominant. Thus, an amplitude variation in travel range is mainly captured by a variation in SIDF. The ratio between the FRF and SIDF defines the nonlinear model as the uncertain region in Fig. 3.

3.2 Motivation

The following constraint, in the closed-loop BW, and objective function are required while maximizing the BW:

$$\text{Constraint: } |T(j\omega)| \in [-1, +1] \text{ dB} \tag{10}$$

$$\text{Objective function: minimize } |S(j\omega)| \tag{11}$$

Based on traditional guidelines by loop shaping, performance and robust stability are often optimized by a high ω_c, high and low open-loop gain $|L|$ respectively below and above ω_c, and a certain range of phase margin within a narrow neighbor around ω_c. Thus, $\angle L$ is paid attention only for robust stability. The traditional guidelines have shortcomings to fulfill (10),(11) for lightly damped systems, because $|L|$ unavoidably remains close to the unity gain within a wide frequency range $\mathbb{F} = [F_1, F_2]$ around ω_c. This challenge is referred to as the unity gain crisis.

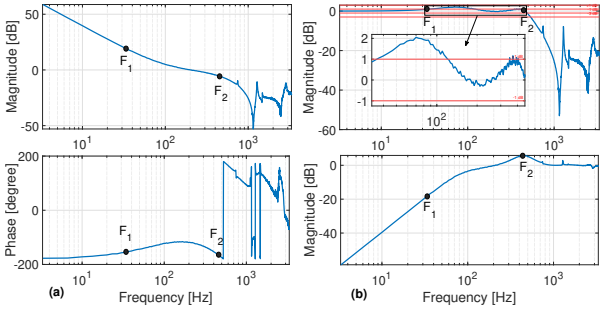


Fig. 4. Linear motion control; (a) Open-loop function, (b) Closed-loop and sensitivity functions.

Motivating example

The linear control below is applied to the nominal FRF:

$$C(j\omega) = C_{PI}(j\omega).C_N(j\omega), C_{PI}(j\omega) = (1 + \frac{\omega_i}{j\omega}).(1 + \frac{\omega_i'}{j\omega}),$$
$$C_N(j\omega) = \frac{(\frac{j\omega}{\omega_m})^2 + \frac{1}{Q_1\omega_m}.j\omega + 1}{(\frac{j\omega}{\omega_m})^2 + \frac{1}{Q_2\omega_m}.j\omega + 1}.\frac{(\frac{j\omega}{\omega_m'})^2 + \frac{1}{Q_1'\omega_m'}.j\omega + 1}{(\frac{j\omega}{\omega_m'})^2 + \frac{1}{Q_2'\omega_m'}.j\omega + 1} \tag{12}$$

with the double integrator C_{PI} and the notch filters C_N. The control parameters are given in Table. 1 regarding the trade-off between high performance and high stability margins. ω_c is thus optimized at 200 Hz.

Table 1. The values of the control parameters

Parameter	Value	Unit	Parameter	Value	Unit
ω_i	$2\pi \times 100$	rad/s	ω_i'	$2\pi \times 100$	$\frac{\text{rad}}{\text{s}}$
ω_m	$2\pi \times 747$	rad/s	ω_m'	$2\pi \times 1287$	$\frac{\text{rad}}{\text{s}}$
Q_1	50		Q_1'	5	
Q_2	0.5		Q_2'	0.5	
ω_r	$2\pi \times 10$	rad/s	ω_f	$2\pi \times 35$	$\frac{\text{rad}}{\text{s}}$
γ	-0.2		ω_h	$2\pi \times 500$	$\frac{\text{rad}}{\text{s}}$
ω_N	$2\pi \times 40$	rad/s	ω_A	$2\pi \times 410$	$\frac{\text{rad}}{\text{s}}$
Q_N	5		Q_A	0.05	
Q_N'	0.5		Q_A'	5	

Fig. 4 depicts the shaped L based on traditional loop-shaping guideline and the resulting S, T. The unity gain crisis exists within the relatively wide frequency range $\mathbb{F} = [33, 443]$ Hz. The non-flat $|T|$ and the concavity on $|S|$ below ω_c are against (10),(11).

4. NEW GUIDELINE IN LOOP SHAPING

Admissible regions are obtained to incorporate (10),(11).

Theorem 1. Let the control structure be given by Fig. 1 ($\mathcal{M} = 1$, $\mathcal{C} = 1$), and let the open-loop L be represented by $\rho e^{j\theta}$, $\rho \in \mathbb{R}_{++}, \theta \in \mathbb{R}$. For each ρ, the open-loop phase requirement θ^* to achieve $|T| = p$, $p \in \mathbb{R}$, is obtained by:

$$\theta^* = \arccos(D), D = -\frac{0.5}{\rho} - 0.5\rho(\frac{p^2 - 1}{p^2}) \tag{13}$$

and it is feasible if $D \in [-1, 1]$ holds.

Proof: Given the desired open-loop $L^* := \rho e^{j\theta^*}$, the additional phase requirement will be $\hat{\theta} = \theta^* - \theta$. The Cartesian representation $L = L_r + jL_i$ is considered. The equality $|T| = p$ is therefore expanded as follows using (6):

$$\frac{|L^*|}{|1+L^*|}=p \Rightarrow \frac{\rho}{|1+Le^{j\hat{\theta}}|}=p \Rightarrow \sqrt{L_r^2+L_i^2}= p.\sqrt{1+2L_r\cos\hat{\theta}-2L_i\sin\hat{\theta}+L_r^2+L_i^2} \Rightarrow \Rightarrow \cos\theta^*=-0.5\frac{1}{\rho}-0.5\rho.(\frac{p^2-1}{p^2}) \quad (14)$$

Formulation (13) is derived by taking arccos from (14). □

Corollary 2. Following Theorem 1, the phase requirement $\theta^* \in [\theta_m^*, \theta_M^*]$ for $|T|=p$, $p \in [p_m, p_M]$ is obtained by:

$$\theta_m^* = \arccos\left(-0.5\frac{1}{\rho}-0.5\rho.(\frac{p_M^2-1}{p_M^2})\right) \quad (15a)$$

$$\theta_M^* = \arccos\left(-0.5\frac{1}{\rho}-0.5\rho.(\frac{p_m^2-1}{p_m^2})\right) \quad (15b)$$

and they are feasible if $D \in [-1,1]$ holds for $p=p_m, p_M$.

Proof: Analytical formulation (13) is decreasing with p. □

Fig. 5 visualizes analytical formulation (15) for $p \in [-1,1]$.

Corollary 3. Following Theorem 1 and Corollary 2, the required phase modification $\hat{\theta}$ for a system with deterministic FRF P at each ω is calculated by:

$$\hat{\theta}(\omega)=\theta^*(\omega)-\theta(\omega) \quad (16)$$

with θ^* from (15) and θ denoting $\angle L$ for given C and K_P.

Proof: Given that $L(\omega)=\rho(\omega)e^{j\theta(\omega)}$ and $L^*(\omega)=\rho(\omega)e^{j\theta^*(\omega)}$, (15) is applied at each ω. □

Next, the formulas are extended to uncertain FRF, $\mathcal{M} \neq 1$.

Theorem 4. Let the control structure be given by Fig. 1 ($\mathcal{M}=\eta e^{j\delta}$, $\mathcal{C}=1$). The dynamics' gain and phase are bounded as $\eta \in [\underline{\eta}, \overline{\eta}]$, $\underline{\eta} \in (0,1] \subset \mathbb{R}, \overline{\eta} \in [1,\infty) \subset \mathbb{R}$ and $\delta \in [\underline{\delta}, \overline{\delta}]$, $\underline{\delta} \in (-\infty, 0] \subset \mathbb{R}, \overline{\delta} \in [0,\infty) \subset \mathbb{R}$. Given $L=\varrho e^{j\vartheta}$, $\varrho \in \mathbb{R}_{++}, \vartheta \in \mathbb{R}$, the conserved phase bounds $\vartheta^* \in [\vartheta_m^*, \vartheta_M^*]$ for $|T|=p$, $p \in [p_m, p_M]$ are obtained by:

$$\vartheta^* \in [\vartheta_m^*, \vartheta_M^*],\ \vartheta_m^*=\boldsymbol{\vartheta_m^*}-\underline{\delta}, \vartheta_M^*=\boldsymbol{\vartheta_M^*}-\overline{\delta} \quad (17a)$$

$$\boldsymbol{\vartheta_m^*}=\arccos\left(-0.5\frac{1}{\boldsymbol{\varrho}}-0.5\boldsymbol{\varrho}.(\frac{p_M^2-1}{p_M^2})\right), \quad \boldsymbol{\varrho}=\max(\min(\frac{p_M}{\sqrt{p_M^2-1}},\overline{\varrho}),\underline{\varrho}), \underline{\varrho}=\rho.\underline{\eta}, \overline{\varrho}=\rho.\overline{\eta} \quad (17b)$$

$$\boldsymbol{\vartheta_M^*}=\arccos\left(-0.5\frac{1}{\underline{\varrho}}-0.5\underline{\varrho}.(\frac{p_m^2-1}{p_m^2})\right) \quad (17c)$$

Proof: A robust region against $\mathcal{M}$ is needed for the phase:

Case (A) $0<p\leq 1$: θ_M^* is increasing with ρ. Hence, it is sequentially conserved as $\boldsymbol{\vartheta_M^*}$ and ϑ_M^* against η and δ.

Case (B) $p>1$: The Hessian of θ_m^* is negative w.r.t ρ with the extremum $\rho=\frac{P_M}{\sqrt{P_M^2-1}}$. Hence, it is sequentially conserved as $\boldsymbol{\vartheta_m^*}$ and ϑ_m^* against η and δ. □

Fig. 5 visualizes the nominal and robust regions.

Corollary 5. Following Theorem 4, required phase modification $\hat{\vartheta}$ for uncertain FRF $\mathcal{P}$ at each ω is given by

$$\hat{\vartheta}(\omega)=\vartheta^*(\omega)-\theta(\omega) \quad (18)$$

with ϑ^* from (17) and θ denoting $\angle L$ for given C and K_P.

Proof: Given that $L(\omega)=\varrho(\omega)e^{j\vartheta(\omega)}$ and $L^*(\omega)=\varrho(\omega)e^{j\vartheta^*(\omega)}$, (17) is applied at each ω. □

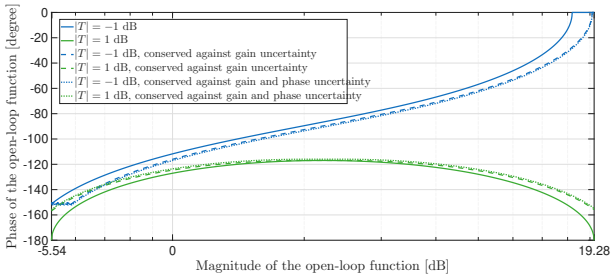


Fig. 5. Conserved bounds for $\underline{\eta}=0.9, \overline{\eta}=1.1, \underline{\delta}=\overline{\delta}=1°$.

Remark 6. The robust region in Theorem 4 returns:

$$\text{Conserved constraint: } |T(j\omega)| \in \mathbf{T}(j\omega), \quad \mathbf{T}(j\omega)=[\underline{T}(j\omega), \overline{T}(j\omega)] \subset [-1,+1] \text{ dB} \quad (19)$$

such that (10) holds in the worst cases of η and δ.

Next, two remarks are given to include (11) in shaping $\angle L$.

Remark 7. Using (6), regions (10),(19) in $|S|$ plane are:

$$\text{Nominal bounds: } |S(j\omega)| \in \mathbf{S}^{\pm 1}(j\omega), \quad \mathbf{S}^{\pm 1}(j\omega)=[\underline{S}^{\pm 1}(j\omega), \overline{S}^{\pm 1}(j\omega)] \text{ dB} \quad (20a)$$

$$\text{Conserved bounds: } |S(j\omega)| \in \mathbf{S}(j\omega), \quad \mathbf{S}(j\omega)=[\underline{S}(j\omega), \overline{S}(j\omega)] \subset \mathbf{S}^{\pm 1} \quad (20b)$$

Remark 8. $\angle L$ is a key in $|S|$ within $\mathbb{F}$ since $|L| \approx 0$ dB. Based on (6),(7), any phase lead (lag) in L reduces (increases) $|S|$. Thus, Corollaries 3,5 are utilized such that any phase lag is avoided.

New loop-shaping guideline for motion control design:

(1) Increase the open-loop gain in open-loop BW (by, e.g, integration) and ω_c.
(2) For the deterministic or uncertain case, $\mathcal{M}=1$ or $\mathcal{M} \neq 1$, go to step 3 or 4 and skip the other step.
(3) Apply Corollary 3 and Remark 8 in the critical range $\mathbb{F}$ to obtain the required additional phase range in L.
(4) Apply Theorem 4 and Remark 8 in the critical range $\mathbb{F}$ to obtain the required additional phase range in L.
(5) Realize the additional phase in $\angle L$ by designing $\mathcal{C}$.
(6) Repeat steps 1 to 5 as long as $\mathcal{C}$ is feasible.

Hence, $\mathcal{C}$ needs to provide phase lead without altering gain.

5. NONLINEAR MOTION CONTROL DESIGN

The actuator operates in 25% of its stroke. Thus, the uncertain region on FRF is assumed to shrink by 25%. The motivating example in Section 3.2 is considered.

Fig. 6 shows the nominal (by Corollaries 2,3) and robust (by Theorem 4 and Corollary 5) regions to shape $\angle L$ in $\mathbb{F}$. $\mathbb{F}'=[F_1', F_2'] \subseteq \mathbb{F}, F_1'=F_1, F_2'=334$ denotes the maximum range where phase shaping is feasible.

Figs. 7,8 depict how metrics (10),(11) are expected to be met. The boundaries for the nominal and worst-case scenarios (respectively $\mathcal{M}=1, \mathcal{M} \neq 1$) are calculated by Remarks 6,7. The bounds in the robust design are conserved compared to the non-robust design to guarantee performance for $\mathcal{M} \neq 1$. (10) is violated by linear control. Moreover, a possibility for improvement in (11) is seen.

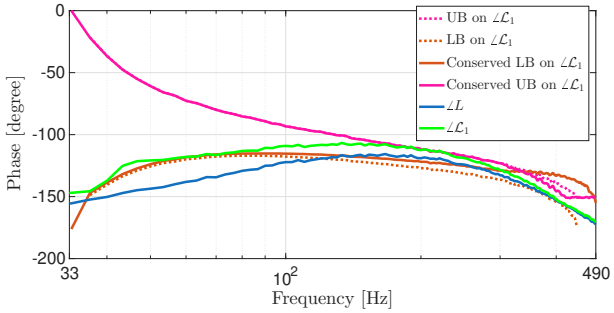


Fig. 6. Required ranges and linear and nonlinear phase.

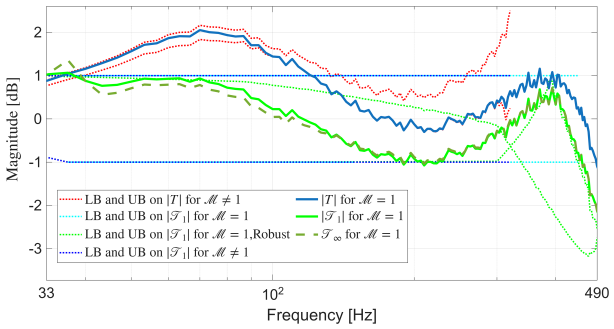


Fig. 7. The ranges on complementary sensitivity function.

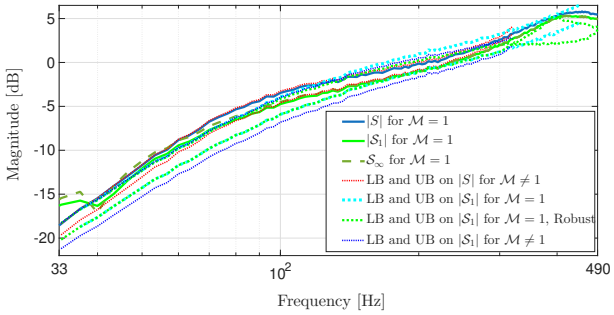


Fig. 8. The ranges on sensitivity function.

5.1 CgLp reset control design

CgLp reset control is considered as $\mathcal{C}$. The high-order harmonics usually cause multiple-resets at frequency. Shaping filter C_s helps avoid multiple-resets and let SIDF-based analysis be valid. An intuitive and systematic scheme is presented for shaping filter design.

$\mathcal{R}_r$ is not activated if $\angle C_s = \angle\mathcal{R}_{\text{bl}}$, intuitive from (2) as e'' and $\boldsymbol{u}$ crosses zero the same time. Hence, $\mathcal{R} = \mathcal{R}_{\text{bl}}$ and no higher-order harmonics are generated. On the other hand, the phase advantage of $\mathcal{R}$ is fully available if $\angle C_s = 0$. The intuitive and practical shaping filter design is given as:

(1) Set $\angle C_s = \angle\mathcal{R}_{\text{bl}}$.
(2) Specify $\mathbb{F}' = [F_1', F_2']$ where reset control is needed.
(3) Make $\angle C_s \geq 0$ in $\mathbb{F}'$. One notch and anti-notch filter around F_1' and F_2', and one lead filter are suggested.
(4) Tune the parameters of the previous step to keep $\angle\mathcal{C}_1$ within the region from new loop-shaping guideline.

The shaping filter is thus given by:

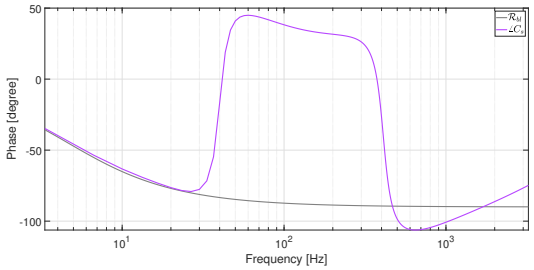


Fig. 9. The phase of the designed shaping filter

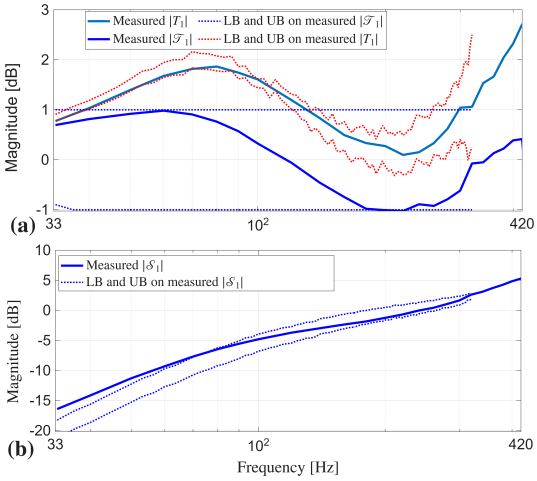


Fig. 10. Measured performance metrics.

$$\mathcal{C}_s(j\omega) = \frac{1}{j\frac{\omega}{\omega_r'}+1}.\frac{(\frac{j\omega}{\omega_N})^2+\frac{1}{Q_N.\omega_N}.j\omega+1}{(\frac{j\omega}{\omega_N})^2+\frac{1}{Q_N'.\omega_N}.j\omega+1}.$$
$$(j\frac{\omega}{\omega_h}+1).\frac{(\frac{j\omega}{\omega_A})^2+\frac{1}{Q_A.\omega_A}.j\omega+1}{(\frac{j\omega}{\omega_A})^2+\frac{1}{Q_A'.\omega_A}.j\omega+1} \tag{21}$$

The parameters of the CgLp reset control are selected as in Table. 1. Fig. 9 depicts $\angle C_s$ which aligns with the presented steps for shaping filter design.

Fig. 6 shows the designed CgLp reset control realizes the phase requirement within most of $\mathbb{F}'$. $\angle\mathcal{L}_1$ lies in most of both nominal (non-robust) and robust regions while $\angle L$ stays out of the required nominal and robust region in $[37, 120]$ Hz and $[37, 131]$ Hz. No multiple-resets occurs.

Figs. 7,8 show $\mathcal{T}_1, \mathcal{S}_1$ are kept by the conserved bounds as long as $\mathcal{L}_1$ is located in the robust region except at low frequency as CgLp control is not perfectly constant in gain. $\mathcal{S}_\infty, \mathcal{T}_\infty$ are plotted to let trust on SIDF-based design. It is expected that the dotted red and dark blue lines encounter the measured $|\mathcal{S}_1|$,$|\mathcal{T}_1|$ according to Theorem 4.

6. EXPERIMENTAL RESULTS

Fig. 10(a) depicts the measured $|\mathcal{T}_1|$ with travel range of 10 μm. (10) is satisfied in $\mathbb{F}'$. Fig. 10(b) shows the measured $|\mathcal{S}_1|$ is located in the expected region except for low frequency, which could be from system noise and slight mismatch between $|\mathcal{S}_\infty|$ and $|\mathcal{S}_1|$ in Fig. 8.

Fig. 11 depicts the triangular tracking response with 25% of the full stroke. Regarding (10), the designed nonlinear control is robust against the plant's nonlinearity while the

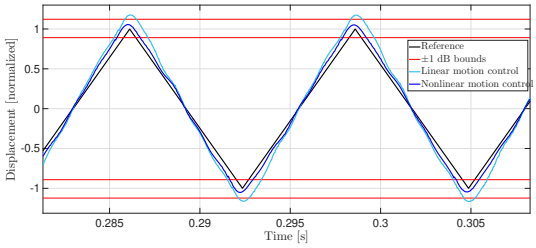


Fig. 11. Triangular tracking at 80 Hz. Phase compensated. linear control with the same ω_c violates the ±1 dB bounds.

7. CONCLUSION

The open-loop phase is critical for performance within a wide range of frequency for motion control design of piezo-actuated positioners. New loop-shaping guideline was presented by rigorous analytical formulations. The guidelines were extended to nonlinear systems. An effective reset control design was provided by presenting a practical and intuitive methodology for shaping filter design.

ACKNOWLEDGEMENTS

The authors express their sincere gratitude to both Mathias Winter, Head of Piezo System & Drive Technology, and Dr.-Ing. Simon Kapelke, Head of Piezo Fundamental Technology, from Physik Instrumente (PI) SE & Co. KG, for their invaluable collaboration in providing technical insights concerning the system and its applications.

DECLARATION OF GENERATIVE AI AND AI-ASSISTED TECHNOLOGIES IN THE WRITING PROCESS

The author(s) used ChatGPT in order to improve the writing style. After that, the author(s) reviewed and edited the content as needed and take(s) full responsibility for the content of the publication.

REFERENCES

Alferink, D., Fey, R.H., Van De Wouw, N., and Heertjes, M.F. (2025). Hysteresis in motion control systems: a frequency-domain analysis on higher harmonics. In *2025 ACC*, 5073–5078. IEEE.

Beker, O., Hollot, C.V., and Chait, Y. (2002). Plant with integrator: an example of reset control overcoming limitations of linear feedback. *IEEE TAC*, 46(11), 1797–1799.

Clegg, J.C. (1958). A nonlinear integrator for servomechanisms. *Trans of the American Institute of Electrical Engineers, Part II: Applications and Industry*, 77(1), 41–42.

Esbrook, A., Tan, X., and Khalil, H.K. (2012). Control of systems with hysteresis via servocompensation and its application to nanopositioning. *IEEE Trans on Control Systems Tech*, 21(3), 725–738.

Guo, Y., Wang, Y., and Xie, L. (2009). Frequency-domain properties of reset systems with application in hard-disk-drive systems. *IEEE Trans on Control Systems Tech*, 17(6), 1446–1453.

Heertjes, M., van Den Eijnden, S., and Sharif, B. (2023). An overview on hybrid integrator-gain systems with applications to wafer scanners. In *2023 IEEE ICM*, 1–8. IEEE.

Heertjes, M., Gruntjens, K., Van Loon, S., Van de Wouw, N., and Heemels, W. (2016). Experimental evaluation of reset control for improved stage performance. *IFAC-PapersOnLine*, 49(13), 93–98.

Hosseini, S.A., Quinten, F.R., van Eijk, L.F., Kostic, D., and HosseinNia, S.H. (2025). Frequency domain design of a reset-based filter: An add-on nonlinear filter for industrial motion control. *arXiv preprint arXiv:2507.01491*.

Hou, X., Dastjerdi, A.A., Saikumar, N., and Hosseinnia, S.H. (2020). Tuning of 'constant in gain lead in phase (cglp)'reset controller using higher-order sinusoidal input describing function (hosidf). In *2020 ANZCC*, 91–96. IEEE.

Karbasizadeh, N., Dastjerdi, A.A., Saikumar, N., and HosseinNia, S.H. (2022). Band-passing nonlinearity in reset elements. *IEEE Trans on Control Systems Tech*, 31(1), 333–343.

Nuij, P.W.J.M. (2007). *Higher order sinusoidal input describing functions: extending linear techniques towards non-linear systems analysis*. Ph.D. thesis, TUe.

Ru, C., Liu, X., Sun, Y., et al. (2016). Nanopositioning technologies. *Fundamentals and applications*.

Sabarianand, D., Karthikeyan, P., and Muthuramalingam, T. (2020). A review on control strategies for compensation of hysteresis and creep on piezoelectric actuators based micro systems. *Mechanical Systems and Signal Processing*, 140, 106634.

Saikumar, N., Heinen, K., and HosseinNia, S.H. (2021). Loop-shaping for reset control systems: A higher-order sinusoidal-input describing functions approach. *Control Eng Practice*, 111, 104808.

Schmidt, R.M., Schitter, G., and Rankers, A. (2020). *The design of high performance mechatronics-: high-Tech functionality by multidisciplinary system integration*. Ios Press.

Zhang, X. and HosseinNia, S.H. (2024a). Enhancing the reliability of closed-loop describing function analysis for reset control applied to precision motion systems. *arXiv preprint arXiv:2412.00502*.

Zhang, X. and HosseinNia, S.H. (2024b). Identifying two-reset conditions for closed-loop sinusoidal input reset control systems. In *2024 20th IEEE/ASME International Conf on MESA*, 1–6. IEEE.

Zhang, X. and HosseinNia, S.H. (2025). Enhancing reset control phase with lead shaping filters: Applications to precision motion systems. *arXiv preprint arXiv:2503.15020*.

Zhao, G., Nešić, D., Tan, Y., and Hua, C. (2019). Overcoming overshoot performance limitations of linear systems with reset control. *Automatica*, 101, 27–35.

Zhao, G., Nešić, D., Tan, Y., and Wang, J. (2013). Open problems in reset control. In *52nd IEEE CDC*, 3326–3331. IEEE.

Zhong, J. and Yao, B. (2008). Adaptive robust precision motion control of a piezoelectric positioning stage. *IEEE Trans on Control Systems Tech*, 16(5), 1039–1046.